Journal of Magnetic Resonance 204 (2010) 333–339

Contents lists available at ScienceDirect

Journal of Magnetic Resonance

journal homepage: www.elsevier.com/locate/jmr

Communication

Implementation equations for HS_n RF pulses

Yasvir A. Tesiram

Oklahoma Medical Research Foundation, 825 NE 13th St, OKC, OK 73104, USA

ARTICLE INFO

Article history:
Received 22 January 2010
Revised 22 February 2010
Available online 25 February 2010

Keywords:
Stretched hyperbolic secant
Implementation equations
Adiabatic decoupling

ABSTRACT

Implementation equations for the family of stretched hyperbolic secant (HS_n) pulses are derived in the linear adiabatic range for inversion of spins. These master equations provide convenience relations for relating the peak amplitude RF_{max} of the pulse to the frequency sweep (*bwdth*) range of the pulse and its duration T_p. The bandwidth of the pulse can also be related to the effective coverage (bw_{eff}) of the pulse to a defined or chosen spectral region. The choice of pulse determined by the use of these derived expressions guarantees uniform inversion to a prescribed efficiency across the selected spectral region. The performance of HS_n pulses in determining the cut-off region between spectral regions was also examined. It is found that beyond a unique T_p*bwdth* product no additional gain may be obtained by extending pulse durations for a chosen *bwdth* of pulse. An example of practical implementation of the inversion pulses is presented for adiabatic decoupling using HS_7 and HS_8 pulses. It is shown that despite added B_1 inhomogeneity in the form of additional amplifier power to 400% from optimal, these pulses can still yield reproducible decoupled spectra.

1. Introduction

The hyperbolic secant (HS) amplitude/frequency waveform [1] is widely used in NMR and MRI for adiabatic broadband or selective inversion or decoupling. Unfortunately a criticism of the pulse is the large peak amplitude (RF_{max}) often required to achieve the desired rotation/s. Modulation functions such as constant/linear (or CHIRP) [2], WURST [3], tanh/tan [4] and numerous others [5] were developed to overcome these limits. All are useful in one manner or another but direct and fair comparison is usually not possible. For example, selectivity profiles defining the cut-off region between two peaks say, may be less than satisfactory and are not readily realized particularly in narrow-band applications. The latter is important in homo-decoupling applications and spectral region selection in crowded spectra as well as slab selection in 3D magnetic resonance imaging applications. While due consideration should be given to all pulses touted to behave adiabatically, complete, accurate and generally applicable methods of implementation into pulse sequence programs still remains a problem because of the difficulty in solving the Bloch equations analytically for any arbitrary input function. Numerical solution of the Bloch equations for an arbitrary waveform during execution of a pulse sequence program may also be feasible. However, when the number of digitization points *np*, in a waveform is large (e.g. >1000 points) calculation may take the order of seconds or more. Moreover, target efficiencies such as the level of inversion have to be determined usually requiring recursive algorithms and in these cases more programming effort is required for failsafe operation. An alternative strategy is the creation of a database of numerically optimized pulses [6,7] but the draw-back is that tables are discrete increments of some parameter of the pulse and so general applicability becomes a problem of finding the closest match from prebuilt input waveforms. Having available a set of simple equations relating the operating parameters of the pulse to the NMR spectrum or image, that are easily programmed for a family of pulses, seems a better approach. The HS_n family [8] meets this criterion. But, there are no implementation equations nor analytical solutions readily realized for the plethora of applications nor combinations of duration, spectral coverage, peak amplitudes, or exponent where these pulse may be used.

In previous work [9], universal implementation equations were derived for sech/tanh pulses, where it was shown that linear master equations of the form $(RF_{max}T_p)^2 = m_{RF}\ T_p bwdth + c_{RF}$ could be derived empirically. Relevant pulse parameters of peak amplitude, RF_{max} (kHz), duration T_p (ms), and nominal pulse frequency sweep *bwdth* (kHz) could be determined and easily implemented in pulse sequence programs for error free use of these inversion pulses. The coefficients m_{RF} and c_{RF} are fitting constants. Likewise the parameter relating the chosen spectral bandwidth bw_{eff} to *bwdth* was also found to be linearly proportional and so implementation only really required the spectral width to be set. Equations were also provided for the tanh/tan pulse and a similar strategy could also be used for determining the relevant parameters for other amplitude and frequency swept schemes such as WURST and the like. These pulses were further categorized as "linearly" or "partially"

E-mail address: yasvirtesiram@yahoo.com.au

1090-7807/$ - see front matter © 2010 Elsevier Inc. All rights reserved.
doi:10.1016/j.jmr.2010.02.022

adiabatic and the $T_p bwdth$ product of each was determined to further limit the use of the pulse to be in the linearly adiabatic range.

In this article, numerically derived master equations for the HS_n family are provided, where n is an integer exponent of time in the modulation functions driving the RF pulse. These pulses (or rather these waveforms) have been used extensively, particularly in applications for $T_{1\rho}$ [10], and $T_{2\rho}$ [11,12], contrast generation [13,14], localized spectroscopy [15] and more recently in frequency swept imaging [16]. The latter, however, is a special application of these pulses where variable spin flips are generated in the linear portion of the peak amplitude profile and may be described as the product operator transform of $I_z \rightarrow I_{\pm(x,y)}$ depending on the phase of the pulse. An excellent treatment has been provided for this promising application [17]. It is also possible to use the equations derived here to arrive at the optimal peak amplitude and this is briefly discussed later in the article. Here only the inversion $I_z \rightarrow -I_z$ is treated. It follows that in the absence of any influence of the coupling mechanism between two spins, the transforms, $2I_zS_z \rightarrow -2I_zS_z$, $2I_zS_{\pm(x,y)} \rightarrow -2I_zS_{\pm(x,y)}$ may also be treated with the derived equations. This operating bound is sometimes called the "high power limit". Evolution of spin states due to a reduced coupling constant may be safely neglected for $T_p \leqslant (1/2J)$ ms and $B_1 >> J$ as has been shown previously [18] for HS_1. HS_n can be applied for short durations without violating peak amplitude or duty cycle requirements. The advantage of HS_n pulses is that with increasing n the peak amplitude of the pulse is reduced and so imaging and spectroscopic applications need not be limited by such things as coil/probe limits. In spectroscopy applications, where it is often thought that only short duration pulses lead to efficient excitations relative to longitudinal and spin–spin relaxation, these pulses also can be of short duration. For ease of implementation, universal master equations guaranteeing consistent performance are required.

2. Results and discussion

2.1. Derivation of peak amplitude master equation

The HS_n amplitude B_1, and phase φ functions, were implemented according to [8]

$$B_1(\tau) = \mathrm{RF_{max}}\,\mathrm{sech}(\beta\tau^n) \tag{1}$$

$$\varphi(\tau) = (360T_p bwdth/np)\int_0^{\tau}\int_0^{\tau} B_1^2(\tau)d\tau \tag{2}$$

with $\tau = 2t/T_p$ (ms) and $-1.0 \leqslant t \leqslant 1.0$. Here $bwdth$ is the extent of frequency sweep in kilohertz, np is the number of digitized points, n is an integer exponent in the range 2–8, the truncation factor $\beta = 5.23^n$ and $\mathrm{RF_{max}}$ is the peak amplitude of the pulse in units of kilohertz. To ensure high fidelity of each pulse, $np \geqslant 1024$. Simulations were carried out with the 3×3 rotation matrix of the Bloch equations as described in [19] in the following fashion.

First, the cut-off for partial adiabaticity was determined by searching for the minimum $bwdth$ where the wobbles disappeared from the $\mathrm{RF_{max}}$ profile for $T_p = 1.0$ ms. That is the $T_p bwdth$ product (or R factor) was varied. The maximum range for the $\mathrm{RF_{max}}$ sweep was determined by considering the potential applications of the pulse. In a proton spectrum it is not unusual to find on-resonance square pulse durations of a few micro-seconds. Of course there are a number of variables to consider but maximum peak amplitudes up to ~60 kHz for protons is feasible for some high resolution probes. For higher gyromagnetic nuclei the maximum is usually quite less. To complete the initial search for $T_p bwdth$ range the maximum limit was found so that the operation $I_z \rightarrow -I_z$ was achieved. The limits of simulation vary with n.

Second, $\mathrm{RF_{max}}$ was determined by continuous application of the rotation matrix to initial unit magnetization $I_z = 1.0$ in 2048 $\mathrm{RF_{max}}$ steps. Third, an interpolating polynomial of the profile was created using Mathematica software (Wolfram Scientific, Champaign, Illinois) and then solved for chosen inversion numbers ι_0, where the inversion number represents the percentage inversion as described previously (9). The inversion numbers chosen were in the range $0.90 \leqslant \iota_0 \leqslant 0.99$ providing an extra variable to ensure guaranteed performance of a chosen pulse. The product $T_p bwdth$ was plotted against $(\mathrm{RF_{max}}T_p)^2$ to yield linear plots from which the intercept and slope were determined and plotted against ι_0 to yield the auxiliary equations of [9].

Shown in Fig. 1 are the $\mathrm{RF_{max}}$ profiles of HS_n pulses for a constant $T_p bwdth$ product. It is easy to note that there is a significant improvement in the peak amplitude required to achieve inversion for a chosen exponent. More importantly though, if amplifier

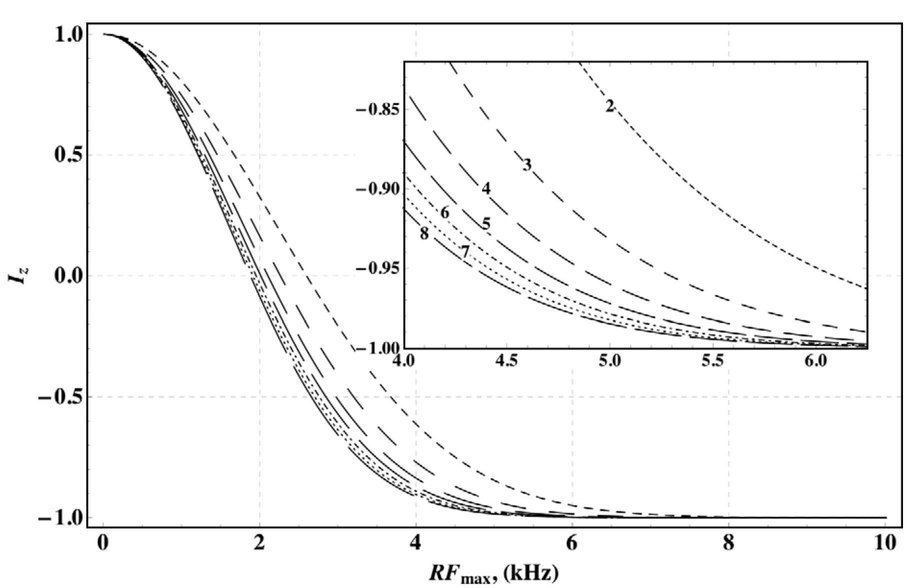

Fig. 1. Peak amplitude profiles for HS_n inversion pulses with $T_p bwdth = 40.0$ ($T_p = 1.0$ ms and $bwdth = 40.0$). An expansion of the region where $\mathrm{RF_{max}} = 4.0$ and 6.25 kHz is plotted showing the lower power required by the various HS_n pulses with increasing n as labeled.

power settings are kept constant such that $RF_{max} \geqslant 8$ kHz, any of the 8 pulses could be used to achieve the same rotation. In addition, the profiles for $n > 5$ only offer marginal improvements in peak amplitude reduction for the same rotation and so in the first instance one would be hard pressed to find any use for HS pulses with $n > 5$. Nevertheless peak amplitudes of this family of pulses may be calculated according to,

$$RF_{max} = T_p^{-1}\sqrt{m_{RF}T_p bwdth + c_{RF}} \tag{3}$$

with

$$m_{RF} = \sqrt{(a_0 + a_1\iota - a_2/(1-\iota))^{-1}} \tag{4}$$

and

$$c_{RF} = (b_0 + b_1\iota - b_2/(1-\iota))^{-1} \tag{5}$$

Curve fitting parameters for each of the HS_n pulses is given in Table 1 and may be substituted into the appropriate equations of [7]. It must be noted that the simulation limits were set in such a way as to reflect the operation of the RF pulse in the linearly adiabatic range. These limits are such that $20 \leqslant T_p bwdth \leqslant 1000$. Thus if a user chooses to operate over a very narrow bandwidth of frequencies, $T_p bwdth$ must be greater than or equal to 20 for the relations given by the fitting parameters of Table 1 to hold. In the case of partially adiabatic pulses, universal relations are even more difficult to establish even with numerical simulation and are outside the scope of this article.

2.2. Determining excitation profile characteristics

Since the inversion profile is symmetric around the chosen RF transmitter frequency, only the point where ι_0 met the chosen setting was recorded. Accordingly the effective bandwidth bw_{eff} is twice the value determined for a pulse of chosen frequency sweep *bwdth*. Effective bandwidth profiles were determined as described for the peak amplitude profiles above using the 3×3 rotation matrix. The relationship between bw_{eff} and *bwdth* is also linear. Determination of an auxiliary function with respect to ι_0 completes the derivation of all functions necessary to define a master equation in terms of the variables, RF_{max}, *bwdth*, bw_{eff}, and T_p.

The response of magnetization inversion across the spectral bandwidth is shown in Fig. 2. Here this is labeled as effective bandwidth (or bw_{eff}) as this is a property of the pulse rather than the chosen spectral bandwidth that may be set by the user in normal operation of a spectrometer. The effective bandwidth coverage is excellent over a large range of frequency offsets except at the edges where deflections from ι_0 are evident. In further simulations for deriving a relationship between *bwdth* and bw_{eff} measurements of bw_{eff} were made in increments of 0.01 from $\iota_0 = 0.900$ to 0.980 but RF_{max} was calculated for $\iota_0 = 0.990$. The difference is called

Table 1
Curve fitting parameters for Eqs. (4) and (5) for calibration of peak amplitude given arbitrary bandwidth and duration HS_n pulses.

n	m_{RF}			c_{RF}		
	a_0	a_1	a_2	b_0	b_1	b_2
1	2.809	−2.695	0.00015	−2.999	2.885	−0.00014
2	13.1721	−12.5443	0.00164557	73.1919	−72.059	−0.000124453
3	23.1589	−22.0563	0.00289193	76.7873	−73.0955	0.00946038
4	30.967	−29.4931	0.00386602	105.994	−100.91	0.0134375
5	36.9702	−35.2109	0.00461509	126.321	−120.215	0.0157604
6	41.6564	−39.6743	0.00519944	146.154	−139.394	0.019002
7	45.3921	−43.2323	0.00566627	148.37	−141.223	0.0167866
8	48.4283	−46.1244	0.00000000	156.039	−147.382	0.0216615

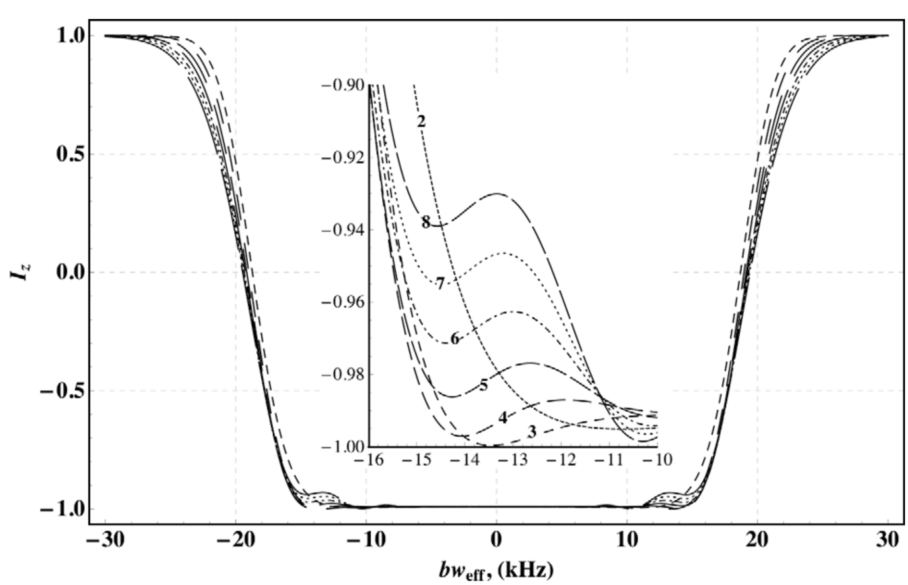

Fig. 2. Effective bandwidth profiles for the HS_n pulses as annotated in the inset for the same pulses used in Fig. 1. With increasing *n*, there is a loss of effective bandwidth coverage at the edge of the effective bandwidth caused by the steeper rise in peak amplitude. Pulses may be truncated at less than 1% of the peak amplitude to overcome the poor response at the edge but at the expense of increased RF_{max}. In broadband applications these losses are of little or no consequence.

$\Delta\iota$. This ensures greater than 96% inversion across the entire spectral bandwidth with 99.5% inversion on-resonance. The plots of Fig. 3 show the intercepts c_{bw}, and slopes m_{bw} of the linear $T_p bw_{eff}$ versus $T_p bwdth$ plots fitted to,

$$m_{bw} = c_0 + c_1/c_2 \cdot \Delta\iota \tag{6}$$

$$c_{bw} = d_0 + d_1/d_2 \cdot \Delta\iota \tag{7}$$

Curve fitting parameters c_n and d_n of Fig. 3 are presented in Table. 2. Determination of the fitting coefficients then enables use of the peak amplitude master Eq. (3) and *bwdth* may be determined by Eq. (8), for a chosen $\Delta\iota$.

$$bwdth = (T_p bw_{eff} - c_{bw})/m_{bw}T_p \tag{8}$$

It is well known that with increasing T_p the selectivity of the inversion profile is inversely proportional. For the simulation results of Fig. 4, the *bwdth* of the RF pulse was set at 40.0 kHz and T_p incremented from 1.0 to 40.0 ms for each of the HS_n pulses. The peak amplitude was calculated using Eq. (3) and the effective bandwidth profile simulated. Interpolating functions were used to calculate the slope of the profile positive edge at the roots of $\iota_0 = 0.5$ and $\iota_0 = -0.5$. Previously, selectivity was defined as $\Delta bw = bwdth - bw_{eff}$. Here a new definition is given where selectivity is redefined as the slope in the range $-0.5 \geqslant \iota_0 \leqslant 0.5$. Thus, for better selectivity $\Delta bw \to \infty$, or rather approaches the asymptote of chosen bw_{eff} because perfectly rectangular profiles across a spectral width are simply not possible. Interestingly, it is observed that beyond a particular $T_p bwdth$ product, no additional gain in selectivity can be achieved. These are plotted as points on Fig. 4. No general relation has been incorporated into Eq. (8) for selectivity but the limits shown in Fig. 4 can be easily incorporated into a pulse sequence program to guide the user in selecting an appropriate

Table 2
Curve fitting parameters of Eqs. (6) and (7) relating the frequency sweep extent of the pulse and its efficiency of response.

n	m_{bw}			c_{bw}		
	c_0	c_1	c_2	d_0	d_1	d_2
1	n/a	n/a	n/a	n/a	n/a	n/a
2	1.16703	0.148477	34.7343	4.91443	−2.69978	32.2359
3	1.09462	0.163382	72.6164	5.63907	−2.33021	33.9993
4	1.06553	0.00328039	2.88295	6.52165	−0.16007	4.48865
5	1.06	0.0605982	136.186	6.90398	0.00331353	56.2083
6	1.05332	0.000368677	7.62293	6.91054	63.5322	1908.44
7	1.07979	−0.00148105	0.891319	3.60916	1.99132	8.28099
8	1.08354	−0.172168	74.0155	3.27327	31.722	98.17

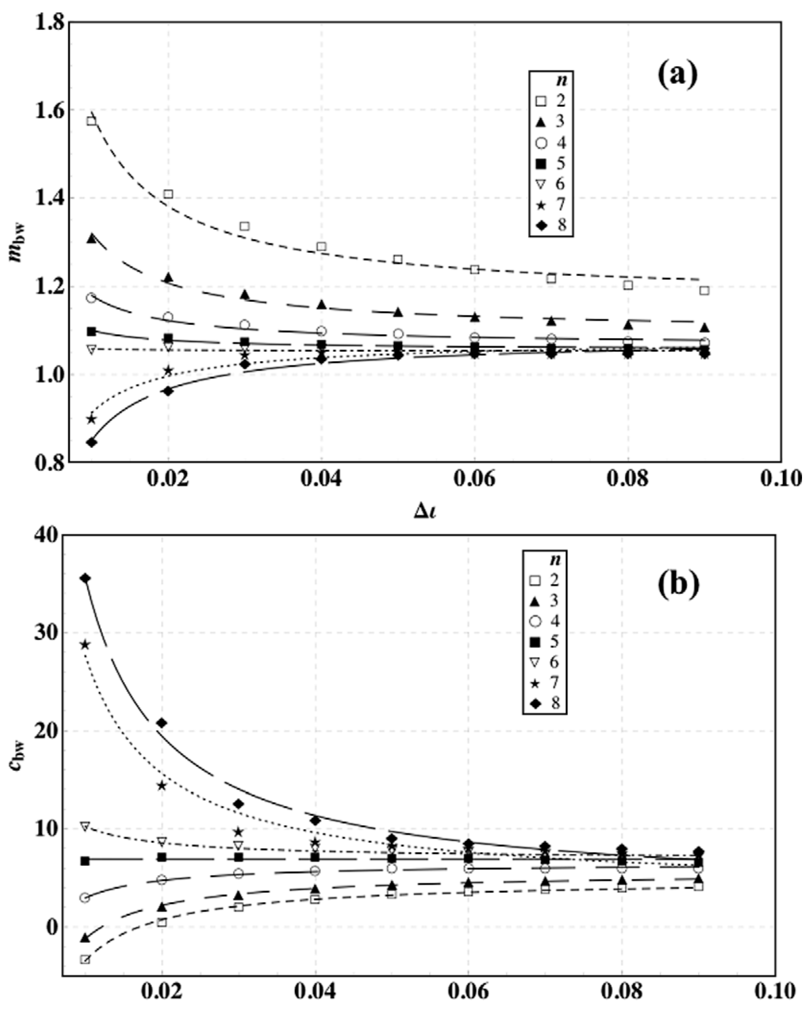

Fig. 3. Plots of the slope m_{bw} (a), and intercept c_{bw} (b) as a function of $\Delta\iota$. The slope and the intercept for each HS_n pulse was determined by curve fitting plots of $T_p bw_{eff}$ versus $T_p bwdth$ by simulating bw_{eff} profiles with the Bloch equations. These are plotted as symbols on the curve fitted lines of Eq. (3). The coefficients of fitting are given in Table 2. The abscissa of the plots are $\Delta\iota = \iota_0 - \iota_{bw}$, where ι_0 is the target inversion number for a desired inversion efficiency (i.e. the number at which RF_{max} was calculated) and ι_{bw} is the inversion number at which bw_{eff} was measured.

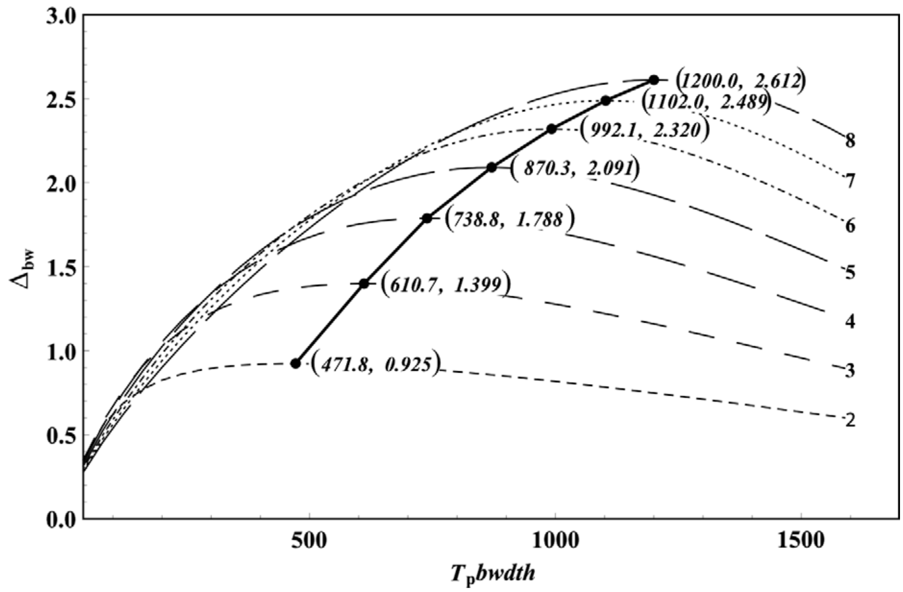

Fig. 4. The behavior of HS_n pulses as a function of increasing duration for constant *bwdth* characterizes a selectivity that is optimal only to certain $T_p bwdth$ limits. The $T_p bwdth$ limit for each of the pulses annotated is shown in brackets. Better selectivity can be achieved with HS_2 than with HS_8 but at the expense of a larger $T_p bwdth$ product. This translates to longer duration pulses in practice.

RF pulse for selective applications. In practical applications selectivity is critical in determining the level of separation between inverted and non-inverted spins.

The accuracy of derived Eqs. (3) and (8) was tested as follows. The effective bandwidth was set at 20.0 kHz. RF pulse *bwdth* was calculated using Eq. (8) for T_p ranging from 1.0 to 10.0 ms. It must be noted here that the first pulse falls in the partially adiabatic range and while the Bloch equation estimate is in error using the automated method with interpolating functions, peak amplitudes may be calculated with Eq. (3). The accuracy will, however, be poor because this represents extrapolation rather than operation within the bounds of numerical simulations. Nevertheless, peak amplitudes calculated for partially adiabatic pulses may be used with caution. With *bwdth* calculated, the resulting HS_n pulses were then used to calculate RF_{max} for a desired level of inversion (in this case $\iota_0 = 0.990$). Since Eq. (3) is compact the calculation takes a negligible amount of time and is ideally suited for "on-the-fly" decision making in pulse sequence programs. For comparison with Eq. (3), Bloch equations were used to generate RF_{max} profiles with peak amplitudes calculated as described in methods section using interpolating functions. Such an operation can take a number of seconds depending on the processor type, *np* and the number of RF_{max} increments etc. The comparison of Eqs. (3) and (8) with Bloch equation simulations are presented in Fig. 5a. Calculated peak amplitudes are in excellent agreement with Bloch equation simulations only deviating by less than 1% for the $T_p bwdth$ range chosen. The correlation coefficient of the straight line fit is 0.9997. As the $T_p bwdth$ product increases, RF_{max} deviation of that calculated from Eq. (3) decreases as well. But as $T_p bwdth$ approaches the partially adiabatic limit, accuracy diminishes. In general the master equation yields highly accurate peak amplitudes for any given $T_p bwdth$ product in the linearly adiabatic range.

In the next test, effective bandwidth profiles were generated using the Bloch equations and compared with the nominal bw_{eff} of 20.0 kHz. Again there is excellent agreement between the chosen effective bandwidth and that calculated using Eq. (8) with deviations less than 1% for $T_p bwdth$ products greater than 20 for all HS_n pulses. These are presented in Fig. 5b. It is also worth noting that the RF pulse is determined by the effective bandwidth. In other words, the spectral width determines the extent of frequency sweep (*bwdth*) for the pulse. Thus comparing Fig. 2 where $T_p bwdth = 40$ with Fig. 5b where $T_p bw_{eff} = 20$ it is clear that having available a set of master equations guarantees practical performance – given that the spectral coverage is similar (i.e. ~20 kHz).

The most common use of adiabatic inversion is in broadband decoupling. Presented in Fig. 6 are spectra from one slice of a ^{15}N HSQC (Fig. 6a) with decoupling of ^{15}N accomplished with HS_8 and HS_7 pulses. An effective bandwidth of 10.0 kHz was chosen and $T_p = 3.0$ ms, thus ensuring an RF pulse operating in the linearly adiabatic range. The frequency sweep extent *bwdth*, was calculated using Eq. (8) yielding 12.0 and 11.9 kHz for HS_7 and HS_8, respectively. Optimal RF_{max} was calculated using Eq. (3), which are 1.68 and 1.65 kHz, respectively. An additional 5–20% of RF_{max} was added to the peak amplitude for HS_8 and HS_7 pulses. Decoupling performance is not compromised even up to 20% increase in RF_{max}. However, the user must be cautioned that adding more power into the sample simply results in sample heating and while line-width increases are not observed for the short acquisition time used for this sample, long acquisition runs on the same sample may lead to decreased performance. This will be true for all such pulses, however.

In Fig. 6c, extreme abuse of amplifier power setting is demonstrated for the HS_7 pulse used for decoupling in ^{15}N HSQC. The decibel units shown here are from that used in Topspin 2.5 software supplied by the instrument manufacturer (Bruker Biospin, GmBH). It is understood that these will be different for the various spectrometers in use. Here a 500 W amplifier was used with −6.0 dB representing full power. In the absence of any peak power checks or duty cycle limits, inadvertent miss-setting of power levels is possible. Thus at 0 dB (~250 W) the user may still observe decoupled peaks in spectra with about 25% loss in signal amplitude from the optimal setting (<9 dB).

3. Experimental

All RF pulses were created using Eqs. (1) and (2), and implemented as either a C program or a Mathematica script for use with Bruker format waveform files. Gradient coherence selected HSQC experiments with sensitivity enhancement [20] were conducted

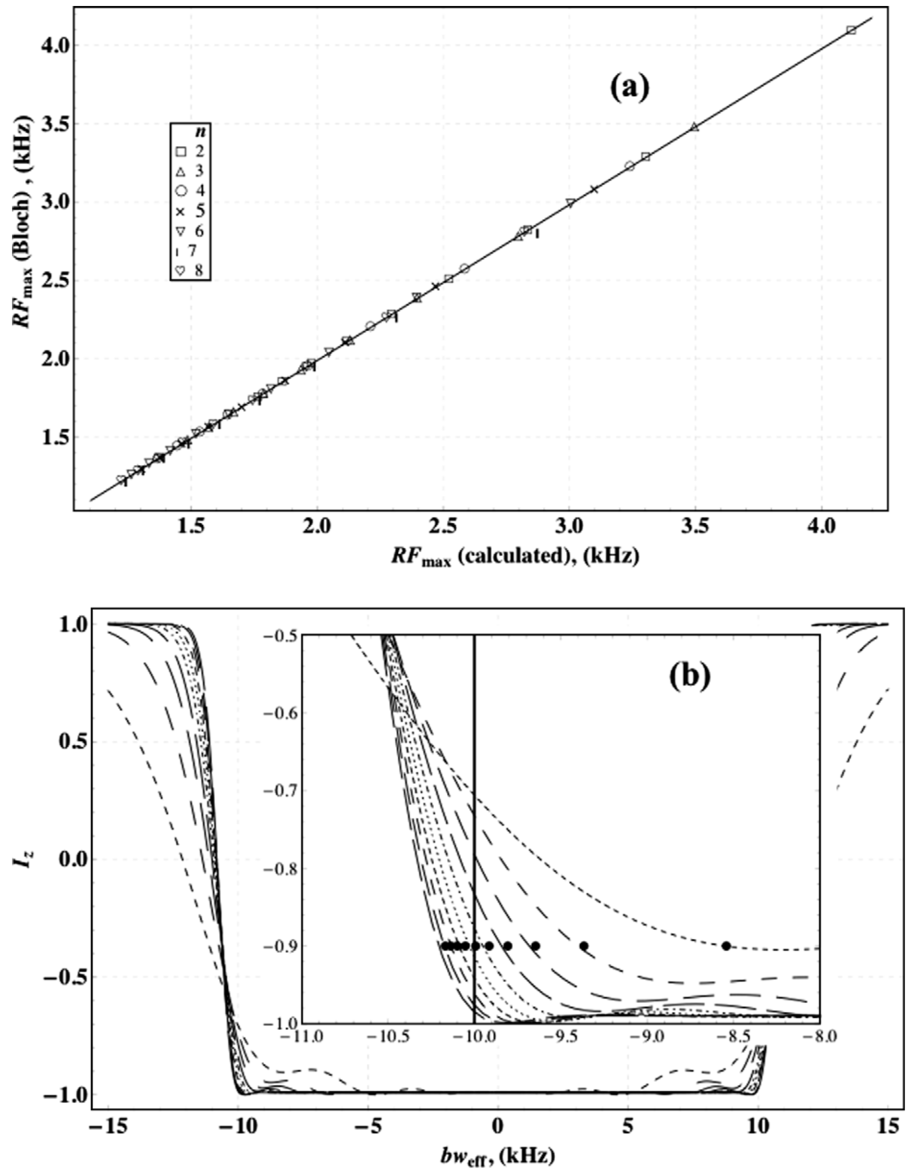

Fig. 5. Accuracy comparison between numerically derived Eq. (3) for (a) effective bandwidth and (b) for $\mathrm{RF_{max}}$ and Bloch equation simulations for the $\mathrm{HS_8}$ pulse as an example. In the inset of plot (a) the effective bandwidth determined by Bloch equation simulation are plotted as points at $\imath_{\mathrm{bw}} = 0.990$. The profiles beginning with $T_{\mathrm{p}} = 1.0$ (right most dashed line) to 10.0 ms (left most plot) in 1.0 ms increments were determined by Bloch equations after calculating the *bwdth* of pulse required for chosen $bw_{\mathrm{eff}} = 20.0$ (solid vertical line) and with $\mathrm{RF_{max}}$ determined by Eq. (3). Thus the divergence of the points from the vertical line represents the divergence of Eqs. (3) and (8) and the approach to partial adiabaticity. Similar plots can be derived for the other HS_n pulses. In addition, the complete plot shows the usual selectivity improvement with increasing T_{p} and this is the case for any RF pulse. In plot (b), the excellent correspondence of Eq. (3) with Bloch equation simulation is demonstrated for all HS_n pulses. Here *bwdth* was determined for a target $\imath_{\mathrm{bw}} = 0.990$ from Eq. (8), and $\mathrm{RF_{max}}$ calculated with Eq. (3) or by simulation. Individual results are plotted as indicated.

on a Bruker 500 MHz NMR spectrometer with a triple resonance XYZ gradient 5 mm probe. The sample used was recombinant ubiquitin (Isotec), 2.5 mg dissolved in 0.5 mL, pH 7.4 buffered H_2O/D_2O (90:10 v/v) solution with a trace amount of NaN_3. The sample was maintained at 295 K for all experiments. The hard 90 degree proton pulse duration for this sample was determined to be 8.3 μs at an amplifier setting of 2.3 dB. The hard 90 degree pulse duration pw_{N} for ^{15}N spins was determined to be 35.0 μs at 2.0 dB. All other conversions were calculated using the following expression;

$$dB = 20\log_{10}(B_{1(\mathrm{ref})}/B_{1(\mathrm{unknown})}) + dB_{\mathrm{ref}} \tag{9}$$

Here $B_{1(\mathrm{ref})} = 1000/4pw_{\mathrm{N}}$ and $B_{1(\mathrm{unknown})} \equiv \mathrm{RF_{max}}$ calculated from Eq. (3). A STUD 112 [21] step phase cycle was directly written into the pulse sequence. In the $F1$ dimension 256 increments were collected and 2048 $F2$ points of the free induction decay. The recycle delay was 1 s and spectra were collected in just over 10 min. All spectra were zero – filled to 4096 × 1024 with sine-bell shifted window functions applied in both dimensions prior to Fourier transform.

4. Conclusion

Adiabatic inversions are of value in NMR spectroscopy and imaging. A major limit of the use of these pulses has been the availability of general relations collecting the variables of such pulses into a closed form expression so that pulse sequence programming and decisions are made easily in some intuitive fashion and realistically related to the spin-system. With the availability of separable

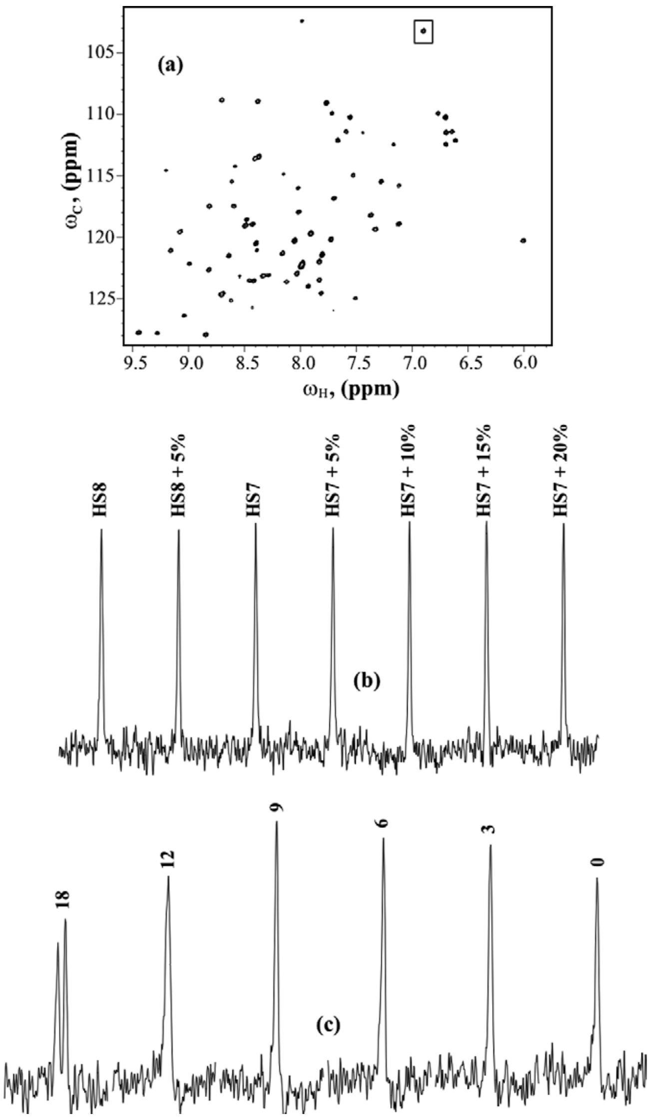

Fig. 6. (a) ^{15}N HSQC spectrum collected with HS_7 used for decoupling with STUD112 cycle showing good decoupling over the entire spectral region. In (b), the decoupled boxed peak is shown with decoupling accomplished with a 3.0 ms HS_8 pulse of *bwdth* = 11.9 kHz, with $\iota_0 = 0.990$ and $\iota_{bw} = 0.900$. RF_{max} was calculated using Eq. (3) yielding 1.65 (optimal) and 1.73 (+5%) kHz. For HS_7, the same inversion efficiency target was used and *bwdth* = 12.0 kHz. The increases in RF_{max} correspond to 1.76, 1.85, 1.93 and 2.02 kHz from 5% to 20% of optimal RF_{max}. Clearly decoupling performance is not compromised. The abuse of extreme power miss-setting is demonstrated in (c) with units given in dB units with 0 dB corresponding to ~250 W for the 500 W amplifier used here. With insufficient RF_{max}, *J*-coupling is only partially decoupled. The increase from 18 to 0 dB corresponds to RF_{max} = 1.13, 2.26, 3.19, 4.51, 6.37, 8.99 kHz, i.e. ranging from a 33% underestimate to 435% over estimate.

expressions for RF_{max}, T_p, *bwdth* and bw_{eff} optimal parameters can be determined very quickly with these expressions embedded into pulse sequence programs.

Acknowledgments

The author thanks Dr. J.-Y. Park (University of Minnesota, Center for Magnetic Resonance Research) for cross-checking a set of simulation results. YAT is funded by Grant NIH RO3 - CA133946 and Oklahoma Medical Research Foundation.

References

[1] M.S. Silver, R.I. Joseph, D.I. Hoult, Selective spin inversion in nuclear magnetic resonance and coherent optics through an exact solution of the Bloch-Riccati equation, Phys. Rev. A 31 (4) (1985) 2753–2755.
[2] V.J. Basus, P.D. Ellis, H.D.W. Hill, J.S. Waugh, Utilization of CHIRP frequency modulation with 180 -phase modulation for heteronuclear decoupling, J. Magn. Reson. 35 (1979) 19–37.
[3] E. Kupce, R. Freeman, Optimized adiabatic pulses for wideband spin inversion, J. Magn. Reson. A 118 (1996) 299–303.
[4] P.C.M. van Zijl, T.-L. Hwang, M. O'Neil Johnson, M. Garwood, Optimized excitation and automation for high resolution NMR using *B*1 insensitive rotation pulses, J. Am. Chem. Soc. 118 (1996) 5510–5511.
[5] A. Tannus, M. Garwood, Adiabatic pulses, NMR Biomed. 10 (1997) 423–434.
[6] M.A. Smith, H. Hu, A.J. Shaka, Improved broadband inversion performance for NMR in liquids, J. Magn. Reson. 151 (2001) 269–283.
[7] K. Kobzar, T.E. Skinner, N. Khaneja, S.J. Glaser, B. Luy, Exploring the limits of broadband excitation and inversion pulses, J. Magn. Reson. 170 (2004) 236–243.
[8] A. Tannús, M. Garwood, Improved performance of frequency-swept pulses using offset-independent adiabaticity, J. Magn. Reson. A 120 (1996) 133–137.
[9] Y.A. Tesiram, M.R. Bendall, Universal equations for linear adiabatic pulses and characterization of partial adiabaticity, J. Magn. Reson. 156 (2002) 26–40.
[10] S. Michaeli, D.J. Sorce, C.S. Springer Jr., K. Ugurbil, M. Garwood, $T_{1\rho}$ MRI contrast in the human brain: Modulation of the longitudinal rotating frame relaxation shutter-speed during and adiabatic RF pulse, J. Magn. Reson. 181 (2006) 135–147.
[11] S. Michaeli, H. Gröhn, O. Gröhn, D.J. Sorce, R. Kauppinen, C.S. Springer Jr., K. Uğurbil, M. Garwood, Exchange-influenced $T_{2\rho}$ contrast in human brain images measured with adiabatic radio frequency pulses, Magn. Reson. Med. 53 (2005) 823–829.
[12] K.T. Jokivarsi, J.-P. Niskanen, S. Michaeli, H.I. Gröhn, M. Garwood, R.A. Kauppinen, O.H. Gröhn, Quantitative assessment of water pools by $T_{1\rho}$ and $T_{2\rho}$ MRI in acute cerebral ischemia of the rat, J. Cereb. Blood Flow Metab. 29 (2009) 206–216.
[13] A. Sierra, S. Michaeli, J.-P. Niskanen, P.K. Valonen, H.I. Gröhn, S. Ylä-Herttuala, M. Garwood, O.H. Gröhn, Water spin dynamics during apoptotic cell death in glioma gene therapy probed by $T_{1\rho}$ and $T_{2\rho}$, Magn. Reson. Med. 59 (2008) 1311–1319.
[14] S. Michaeli, T.C. Burns, E. Kudishevich, N. Harel, T. Hanson, D.J. Sorce, M. Garwood, W.C. Low, Detection of neuronal loss using $T_{1\rho}$ MRI assessment of ^1H_2O spin dynamics in the aphakia mouse, J. Neurosci. Methods 177 (2009) 160–167.
[15] J.-Y. Park, M. Garwood, Spin-echo MRI using $\pi/2$ and π hyperbolic secant pulses, Magn. Reson. Med. 61 (2009) 175–187.
[16] D. Idiyatullin, C. Corum, J.-Y. Park, M. Garwood, Fast and quiet MRI using a swept radiofrequency, J. Magn. Reson. 181 (2006) 342–349.
[17] D. Idiyatullin, C. Corum, S. Moeller, M. Garwood, Gapped pulses for frequency-swept MRI, J. Magn. Reson. 193 (2008) 267–273.
[18] M.R. Bendall, Heteronuclear *J* coupling precession during spin-lock and adiabatic pulses. Use of adiabatic inversion pulses in high-resolution NMR, J. Magn. Reson. A 116 (1995) 46–58.
[19] M.R. Bendall, T.E. Skinner, Comparison of use of vector and quantum representations of *J*-coupled spin evolution in an IS spin system during RF irradiation of one spin, J. Magn. Reson. 142 (2000) 329–351.
[20] L.E. Kay, P. Keifer, T. Saarinen, Pure absorption gradient enhanced single quantum correlation spectroscopy with improved sensitivity, J. Am. Chem. Soc. 114 (1992) 10663–10665.
[21] T.E. Skinner, M.R. Bendall, A phase-cycling algorithm for reducing sidebands in adiabatic decoupling, J. Magn. Reson. 124 (1997) 474–478.